Integration of Rotor Aerodynamic Optimization with the Conceptual Design of a Large Civil Tiltrotor

C. W. Acree, Jr.
Cecil.W.Acree@nasa.gov
NASA Ames Research Center, Moffett Field, California 94035, USA

Abstract

Coupling of aeromechanics analysis with vehicle sizing is demonstrated with the CAMRAD II aeromechanics code and NDARC sizing code. The example is optimization of cruise tip speed with rotor/wing interference for the Large Civil Tiltrotor (LCTR2) concept design. Free-wake models were used for both rotors and the wing. This report is part of a NASA effort to develop an integrated analytical capability combining rotorcraft aeromechanics, structures, propulsion, mission analysis, and vehicle sizing. The present paper extends previous efforts by including rotor/wing interference explicitly in the rotor performance optimization and implicitly in the sizing.

Notation

A	rotor disk area
b	wing span
c_d	section drag coefficient
c_{do}	section profile drag coefficient
C_T	rotor thrust coefficient, $T/(\rho A V_{tip}^2)$
C_W	rotor weight coefficient, $W/(\rho A V_{tip}^2)$
D	drag
D_i	induced drag
e	Oswald efficiency factor
FM	figure of merit
L	lift
L/D_e	aircraft lift over equivalent drag, WV/P
M_{tip}	blade tip Mach number
P	power required
P_{ind}	induced power
P_o	profile power
q	dynamic pressure
R	rotor radius
T	rotor thrust
v_i	induced velocity
V	airspeed
V_{br}	aircraft best-range speed
V_{tip}	rotor tip speed
W	gross weight
WE	weight empty
η	propulsive efficiency
κ	induced power factor
ρ	air density
σ	rotor solidity (thrust-weighted)
CRP	Contingency Rated Power
ISA	International Standard Atmosphere
LCTR	Large Civil Tilt Rotor
MCP	Maximum Continuous Power
MRP	Maximum Rated Power (take-off power)
NDARC	NASA Design and Analysis of Rotorcraft
OEI	One Engine Inoperative
OGE	Out of Ground Effect
SFC	Specific Fuel Consumption
SNI	Simultaneous Non-Interfering approach
STOL	Short Takeoff and Landing
VTOL	Vertical Takeoff and Landing

Presented at the AHS Aeromechanics Conference, San Francisco, CA, January 20-22, 2010. *This material is declared a work of the U. S. Government and is not subject to copyright protection.*

Introduction: Integration of Aeromechanics and Sizing

Increasing demands upon rotorcraft performance and efficiency require more sophisticated analyses to be employed early in the design process, including deeper integration of aeromechanics and sizing analyses. This paper illustrates the use of aeromechanics analysis for component optimization, and then application of the results to aircraft sizing and performance analysis with a sizing code. This effort is part of a NASA goal to develop an integrated analytical capability combining rotorcraft aeromechanics, structures, propulsion, mission analysis, and vehicle sizing.

A new design/sizing code, NDARC, has been developed by NASA to enable exploratory design studies of advanced rotorcraft. A technical description of NDARC is given in Ref. 1; the complete theory is documented in Ref. 2. The CAMRAD II aeromechanics code provides a variety of aerodynamic and structural models, applicable to either component (rotor and wing) or total aircraft performance, dynamics, and acoustics analyses. Reference 3 provides a summary of CAMRAD

II capabilities; see Ref. 4 for details of the theory and methods.

In addition to coupling design and aeromechanics, the present paper expands and improves upon previous efforts by including rotor/wing interference explicitly in the aeromechanics analysis and implicitly in the sizing. Analysis of the rotor and wing aeromechanics together with CAMRAD II, coupled with simultaneous rotor and wing sizing by NDARC, moves the research effort further toward a fully coupled systems design process.

Optimization is extended beyond rotor/wing performance to vehicle sizing. Neither an aeromechanics nor a sizing analysis alone will suffice: the two must be coupled to determine the optimum design. The present study is not intended to generate a final, perfect design, but to demonstrate the procedures needed to do so, in the expectation that further technology advances and design requirements may be progressively incorporated into the process as research progresses.

Methods and Approach

NDARC includes performance and weight models of a variety of rotorcraft components and systems (rotor, wing, engine, fuselage, etc.) that are assembled into a complete aircraft model. NDARC is designed for high computational efficiency. Performance is calculated with physics-based models (e.g. rotor momentum theory), with a wide choice of modeling methods (constant, linear and nonlinear) to best match higher-order analyses or test data. The weight models are typically based upon historical weight trends. Any of the component models can be adjusted by technology factors. NDARC also includes a flexible mission model plus point-design performance analyses for sizing. Given a set of component models, NDARC calculates vehicle size, weight and power required for the chosen mission model and performance requirements.

CAMRAD II is a comprehensive rotorcraft analysis code that includes multibody dynamics, nonlinear finite elements, and rotorcraft aerodynamics. CAMRAD II can model separate rotor and wing free wakes, with or without rotor-on-wing, wing-on-rotor, or mutual wing/rotor interference. Only results with no interference or full, mutual wing/rotor interference are presented here. CAMRAD II is well-suited for rotorcraft design optimization where efficient aeromechanics analysis is needed.

The design example used here is the second-generation Large Civil Tiltrotor (LCTR2, Fig. 1), which has been the object of NASA research described in Refs. 5-15. In the present paper, the emphasis is on aerodynamic performance of the wing and rotor as a system. The immediate objective is to better understand the aerodynamic phenomena that drive rotor optimization, specifically the effects of cruise tip speed and wing/rotor interference. Optimization of the complete aircraft can then proceed with greater confidence that the underlying rotor behavior is properly modeled.

The aeromechanics analyses are similar to those of Refs. 11-13. In Refs. 12 and 13, the LCTR2 baseline design was determined by an older sizing code, RC (Ref. 16), and CAMRAD II was used to investigate performance for different design variations from the baseline. Reference 13 reported optimization of LCTR2 rotor tip speed, and Ref. 11 reported the effects of rotor/wing interference for a large military tiltrotor. The level of analysis necessary for proprotor performance optimization was explored in Ref. 17.

The major conceptual addition for the present paper is the coupling of the CAMRAD II aeromechanics analyses to the new NDARC sizing code to determine the minimum vehicle weight over the entire mission, not just best aerodynamic performance. All hover and cruise performance calculations were updated for the present work, using CAMRAD II Release 4.7 and NDARC version 1.1.

The importance of aerodynamic interference on rotor/wing performance has been widely studied. Reference 18 provides a good historical overview of the subject, with a useful bibliography and examples for hover, transition and cruise. Reference 18 also points out the need to optimize rotor twist for favorable wing/rotor interference, not just for isolated rotor performance. Reference 19 discusses optimal wing lift distribution in the presence of rotor/wing interference. The influence of rotor advance ratio on wing performance was studied in Ref. 20; subsequent studies of the effects of advance ratio include Refs. 21 and 22. More recently, Ref. 11 analyzed wing/rotor interference effects for a large tiltrotor.

Outline of sizing procedures

The sizing process can be summarized as follows:

1. An initial design establishes baseline values of empty weight, rotor radius, tip speed, etc.
2. A CAMRAD II model of the isolated rotor calculates rotor performance trades as rotor design parameters are varied. For the LCTR2 example presented here, several performance maps of hover figure of merit versus cruise propulsive efficiency were generated for different cruise tip speeds. The performance curves represent the boundaries of hover/cruise performance trades as the blade twist distribution is varied.
3. The rotor configurations with the best performance—that is, those falling on the outer boundary of the performance map—are then analyzed by CAMRAD II

with a full rotor/wing interference model. This analysis generates a detailed performance model, including equivalent rotor hover and cruise efficiency and wing efficiency in cruise, for each candidate parameter variation.

4. The performance model so generated was supplied to the NDARC sizing code, which sized the aircraft for the specified mission model. The results comprised curves of empty weight, installed power, fuel burn, etc. versus figure of merit and propulsive efficiency. The LCTR2 rotor/wing performance maps were thereby converted into weight/power tradeoff curves for each cruise tip speed.

There are thus three sets of design tradeoffs: cruise vs. hover rotor performance for each cruise tip speed (V_{tip}); rotor vs. wing efficiency, as a function of V_{tip}; and vehicle size, determined by the weight vs. efficiency tradeoff over the entire mission.

At this point, one can select the best design, determined as lowest weight, lowest power, or some other criterion. More generally, the process would be repeated by updating the baseline design, adjusting the rotor model accordingly, and recomputing performance, weight, etc., or else different design parameters (e.g. blade taper or wing span) would be varied. Different technology assumptions (e.g. engine maps or airfoil decks) might also be introduced and the cycle repeated.

The choice of example design parameters analyzed for this paper is explained in more detail in the section "Sizing Analysis". The process described here stops short of a full formal optimization, most obviously because no objective function is specified (other than weight). Because the focus is on research, it is more useful to "unroll" the process to reveal the aerodynamic effects than to terminate with a final design that may obscure important technical insights.

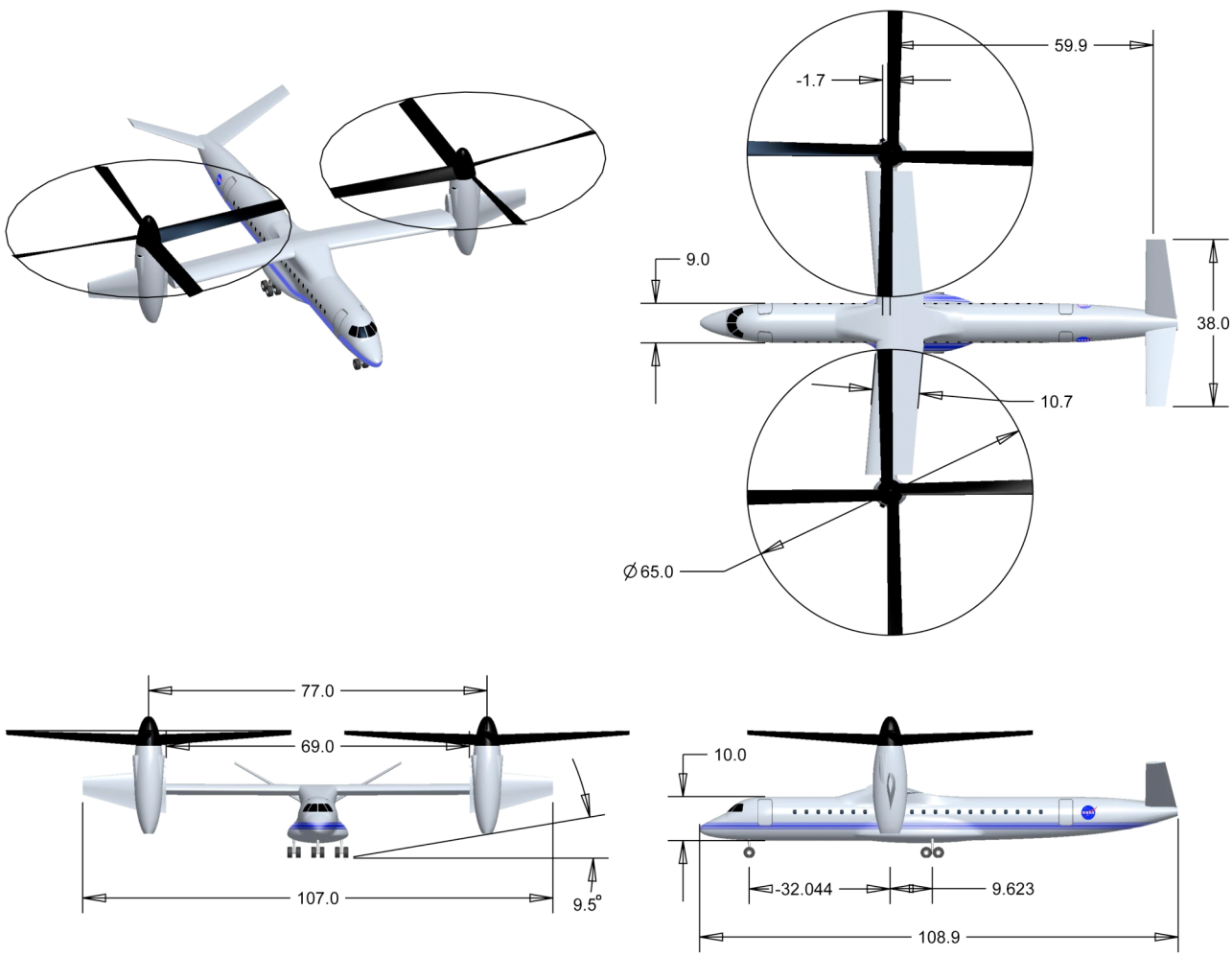

Fig. 1. The NASA Large Civil Tiltrotor, LCTR2 baseline version (dimensions in feet).

LCTR2 Concept Design

The Large Civil Tiltrotor (LCTR), was developed as part of the NASA Heavy Lift Systems Investigation (Ref. 5). The concept has since evolved into the second-generation LCTR2, described in detail in Ref. 13. The LCTR2 design goal is to carry 90 passengers for 1000 nm at 300 knots, with vertical takeoff and landing. Mission specifications and key design values are summarized in Tables 1 and 2 for LCTR2.

Aeroelastic stability (whirl flutter) was examined in Ref. 14. The studies reported in Ref. 13 revealed that turn performance could be a major design driver, with important implications for rotor optimization. Reference 15 subsequently developed criteria for turn performance margins.

The LCTR2 design has four engines for good OEI performance. The engine model assumes advanced engines with a cruise SFC of 0.375 lb/hr/hp. A two-speed transmission ensures that the turbine speed is held constant over different operating conditions for maximum engine efficiency. The combination of a rotor with a wide range of rotational speeds and a multi-speed transmission was demonstrated in principle by the XV-3 (Ref. 23).

Evolution of the LCTR2 concept

The LCTR2 is designed to require only helipads located within existing airport boundaries. The operational concept is to move short- and medium-range air traffic off of the main runways, which would free up such runways for use by greater numbers of larger and longer-range aircraft. The use of large VTOL aircraft would thereby improve the capacity of the airspace system as a whole without requiring construction of new runways or expansion of airport boundaries. The basic design requirements and mission specifications are given in Tables 1 and 2.

The LCTR2 variant presented in Ref. 13 was designed with the RC sizing code; that variant is here designated LCTR2-01. LCTR2-01 was designed with fixed fuselage geometry, dictated by passenger requirements (four abreast), and fixed wingspan and rotor diameter, determined by gate-space limitations. For the final design iteration presented in Ref. 13, the engine size was fixed at 7500 HP. The LCTR2-01 transmission was sized by a 2K/97 (2000-ft ISA + 25°C altitude) operating condition. The fixed airframe geometry and engine size did not seriously limit the design, because those specifications benefited from several previous design iterations.

In contrast, the LCTR2-02 variant described herein was designed using NDARC (Refs. 1 and 2). NDARC is a more advanced design tool than RC, with a more sophisticated rotor performance model and more flexible options for sizing, among other improvements. Relevant features of NDARC are discussed in context in the following sections of this paper.

Table 1. LCTR2-02 mission requirements.

Mission summary
Takeoff + 2 min hover OGE 5k ISA+20°C
Climb at V_{br} (credit distance to cruise segment)
Cruise at V_{br} for at least 1000 nm range, 28k ISA
Descend at V_{br} (no range credit)
1 min hover OGE + landing, 5k ISA+20°C
Reserve (diversion): 100 nm V_{br}, 28k ISA
Reserve (emergency): 30 min V_{br}, 5k ISA+20°C
Operational requirements
One engine inoperative: Category A at 5k ISA+20°C
All-weather operations: CAT IIIC SNI, Free Flight
45-deg banked turn at 80 knots, 5k ISA+20°C, 90% MCP

Table 2. Baseline design values for LCTR2-02.

Design Constraint	Value
Payload (90 pax), lb	19,800
Cruise speed (90% MCP), knots	300
Length, ft	108.9
Wing span, ft	107.0
Wing sweep	−5.0 deg
Rotor radius, ft	32.5
Rotor separation, ft	77.0
Number of blades	4
Precone, deg	6.0
Tip speed, hover, ft/sec	650
Tip speed, cruise, ft/sec	350
Baseline Design	**Result**
Gross weight, lb	103,600
Rotor weight, lb (both rotors)	8113
Wing weight, lb (zero fuel)	7441
Engines and drive train, lb	14,174
Fuselage empty weight, lb	12,875
Mission fuel, lb	16,092
Engine power, hp	4×7489
Rotor solidity	0.128
Rotor taper (tip/root chord)	0.70
Hover C_T/σ	0.163
Cruise C_T/σ	0.0784
Wing area, ft^2	965
Drag D/q, ft^2	34.6

NDARC model and sizing of LCTR2-02

The new features of NDARC were freely exploited for the design of the revised aircraft. The rotor performance model was improved, and the rotor sizing (disk loading) was updated to incorporate maneuvering requirements taken from Ref. 15. The basic airframe geometry was

again fixed, but the transmission was sized to provide a 10% torque margin over the worst-case operating condition (the 2K/97 transmission sizing condition was thus made redundant and was deleted). Engine size was allowed to vary to obtain the best match over all operating conditions. In practice, engine and transmission size were set by the sizing conditions of Table 3, including the 10% margin on the transmission torque. Fuel consumption was calculated for the entire mission of Table 1. Weight empty, including fuel tank size, wing chord, and rotor solidity were then iterated along with engine and transmission size to achieve a converged solution. This yielded a new baseline design, the LCTR2-02, which is slightly lighter than the LCTR2-01, largely through a reduction in fuel burn. The engines, wing and rotor solidity are also slightly smaller. Major LCTR2-02 design values are summarized in Table 2.

Table 3. LCTR2-02 design constraints for sizing.

Minimum Performance	
Max. takeoff weight at sea level standard, 100% MRP	
OEI at 5k ISA+20°C, CRP×110% [1]	
Cruise speed 300 knots at 28k ISA, 90% MCP	
Key Technology Assumptions	
Wing loading, lb/ft^2	107.4
Disk loading, lb/ft^2	15.6
Hover C_W/σ	0.133
Cruise SFC, lb/hr/hp [2]	0.375
Tip speed, hover, ft/sec [3]	650

[1] Approximate OEI trimmed power not at MCP hover
[2] Summary of engine model specifications
[3] Set by assumed future noise requirements

For the sizing examples presented in this paper, most design values were either held fixed and matched to those of the earlier LCTR2-01 design of Ref. 13 (e.g. wing span), or were determined by underlying technology assumptions equivalent to those used in Ref. 13 (e.g. wing loading). For example, the LCTR2-02 airframe geometry was held fixed, with the exception of wing chord, which was adjusted during the sizing analysis to maintain constant wing loading (Table 3).

Mission model

NDARC can analyze a mission as a set of separate flight conditions, specified as individual segments which are combined into a continuous mission with cumulative fuel burn, or as multiple discrete sizing conditions at which one or more performance requirements must be met, or a combination of both. For a tiltrotor, the rotors are trimmed to the appropriate collective, and optionally cyclic, settings to match thrust, torque, flapping, etc. to the current flight condition. The entire aircraft—rotors, wing, tail, fuselage, nacelles, etc.—is trimmed to total lift, drag, and pitching moment. This is done for each mission segment and sizing condition, and weight, power, or other specified design variables are iterated until a converged solution is found.

For this paper, the mission of Ref. 13 was revised to include a 100-nm reserve segment (Table 1). Mission reserves are thus a combination of turboprop and helicopter practice (distance and time, respectively). The rationale is that while a tiltrotor does not need a runway for an emergency landing, a routine weather diversion may require other airport facilities generally equivalent to those for a turboprop or regional jet, hence the 100-nm segment. In emergencies, the LCTR2 can be operated like a helicopter, hence a 30-min time reserve is appropriate.

NDARC has options for splitting segments into sub-segments to better account for fuel burnoff during cruise and performance changes with density altitude during climb and descent. The mission model was checked with the baseline LCTR2 to ensure that the addition or subtraction of sub-segments did not significantly change the gross weight. The criteria was that the change in gross weight must be less than one passenger (0.2% gross weight) and the change in required power less than the same percentage.

In addition to the nominal mission, three sizing conditions were imposed: minimum cruise speed of 300 knots at altitude, OEI hover at 5000-ft ISA +20° C altitude, and maximum gross weight takeoff at sea level standard conditions (Table 3). In practice, an engine failure over the runway or landing pad would result in an immediate vertical landing, and a failure while wing-borne would be treated like any fixed-wing airliner. The critical OEI condition is then at low speed departing the landing site, but not yet converted to airplane mode. Under such conditions, the rotor inflow from even a low forward speed would reduce rotor power required below that for hover. Calculation of the exact worst-case condition would require much more extensive analyses of aeromechanics and handling qualities than are warranted here. For the present study, a 10% power reduction was assumed for OEI hover, implemented as a 10% increase in power available as a practical approximation. Nominal OEI contingency power is assumed to be 4/3 maximum continuous power, so the rotors are trimmed to 4/3×MCP×110% at the design OEI condition.

Sizing Analysis

Determination of optimum cruise tip speed was chosen as the example problem because it strongly and directly affects other critical design parameters. The hover/cruise tip-speed ratio may size either the gearbox or engine (and possibly both) in cruise, depending on flight conditions, rotor performance, and whether a single- or multi-speed

gearbox is used. Hover and cruise tip speeds will also drive the choice of rotor airfoils, and will together determine how rotor twist must be optimized. Cruise tip speed will also affect aeroelastic stability (whirl flutter) and of course rotor frequency placement. It will also determine airfoil design, especially at the tip.

Other design variables, such as wing twist, span, and chord, are also important, but their affects may cascade through the design only weakly or indirectly via fuel burn. For example, wing twist has no direct effect on the rotor design, and a very small affect (if any) on wing weight. Wing twist affects total vehicle size through fuel burn in cruise, not through the direct sizing of any component or subsystem.

For these reasons, it was highly desirable to choose cruise and hover tip speeds early in the design process. Hover tip speed was limited by noise considerations to 650 ft/sec. Previous efforts (Ref. 13) selected a cruise tip speed of 400 ft/sec based on aerodynamic performance, and examined aeroelastic stability (whirl flutter) using that tip speed (Ref. 14). However, those analyses did not utilize a sizing code, so the results did not guarantee an optimum vehicle size. In order to ensure continuity with the earlier results generated by the older RC sizing code, the baseline cruise tip speed reverted to 350 ft/sec for the initial NDARC sizing studies.

For the LCTR2, maximum disk loading is determined by maneuvering requirements, and was fixed at 15.6 lb/ft^2 for the present study; the value is derived from Ref. 15. While a fixed disk loading may not yield the true optimum design, it guarantees that both the maneuver and engine-out requirements of Table 3 will be met. Once the design space has been narrowed by the choice of cruise tip speed, further optimizations of other design variables (e.g. wing twist or disk loading) can proceed with reasonable assurance that the critical requirements will continue to be met.

NDARC is not a general-purpose, multi-parameter optimization code, but a specialized rotorcraft sizing tool specifically intended to reflect accepted rotorcraft design practices and technology assumptions. For example, not all rotor parameters—radius, solidity, disk loading, tip speed, thrust coefficient, etc.—may be varied at once. Some traditional rotor design and performance parameters, such at C_T/σ, will be automatically determined by the values of other parameters; a choice of what to vary and what to hold fixed must be made at the outset. Furthermore, the parameter variations appropriate for a sizing code are not necessarily the same as for an aeromechanics analysis. For example, Ref. 15 varied rotor solidity to determine the maneuvering criteria for LCTR2; in that analysis, weight did not vary. For the NDARC analyses reported here, rotor disk loading was derived from the baseline values of solidity and hover C_T/σ as adjusted to meet the maneuver requirements of Ref. 15 (Table 2), then disk loading was held fixed and radius varied as the weight and power were updated during the sizing. Rotor solidity is then a fallout parameter dependent upon the adjusted values of weight and radius.

Rotor radius is limited by airport gate spacing. Radius was here allowed to vary because earlier studies had settled on a reasonable value as a baseline. A reduction in rotor radius was acceptable, but not an increase (at least not without an increase in wing span for rotor/fuselage clearance, with consequent weight increase and other resulting design changes). Once the aeromechanics and sizing analyses had been coupled and the procedure refined, the optimization process resulted in lower vehicle weight. Given fixed disk loading, the rotor radius was automatically reduced, but only slightly.

CAMRAD II Rotor and Wing Model

The CAMRAD II rotor model of the LCTR2 had five elastic beam elements per blade, with full control-system kinematics, and 15 aerodynamic panels per blade. Blade aerodynamics were modeled as a lifting line coupled to a free-wake analysis. An isolated-rotor, axisymmetric solution was used for hover and cruise performance optimization. The rotor/wing interference model incorporated a wake model for the wing in addition to the rotor wakes. The rotor/wing wake model was developed for the work reported in Ref. 11 and is shown schematically in Fig. 2.

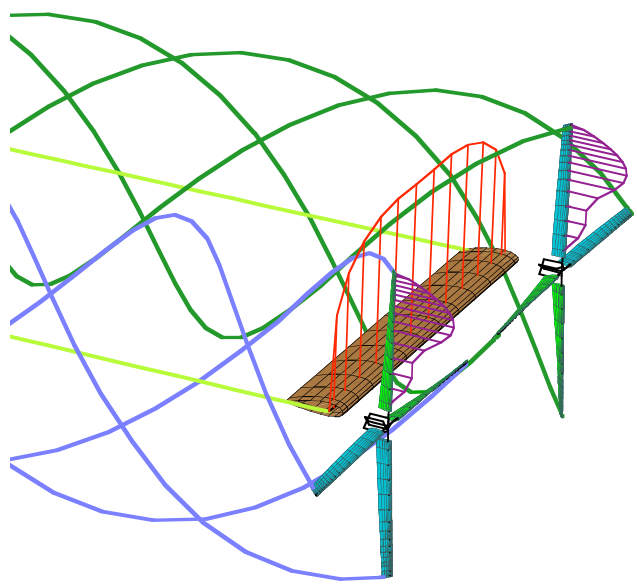

Fig. 2. CAMRAD II rotor and wing wake model (Ref. 11).

Blade- and wing-section aerodynamic properties were read from 2-D airfoil coefficient tables. Rotating, 3-D stall delay was implemented as modifications to the 2-D

aerodynamic table data, based on the analysis of Ref. 24. Fuselage aerodynamics were modeled with an equivalent drag D/q, adjusted to match total wing/body drag computed by CFD analysis.

To simulate advanced airfoils, the rotor airfoil tables were constructed based upon projected improvements beyond existing airfoil capabilities. These projections were based on CFD analysis and modern rotor airfoil trends. The "virtual airfoils" represented by these tables simulate performance levels expected of state-of-the-art, purpose-designed airfoils. The tables were constructed to be generally compatible with XN-series characteristics (Ref. 25), with slight performance improvements consistent with more modern airfoils. The tables used here are documented in Ref. 13.

The main wing is designed with constant chord and 24% thickness, and uses a purpose-designed airfoil (Ref. 9). The tip extensions taper to 35% of the main chord and are set to the same incidence angle as the wing (Ref. 13). The wing and extensions are untwisted. The CAMRAD II wing aerodynamic model used 32 panels, including 7 panels for each tip extension.

For calculations of wing/rotor interactions in cruise, the wing incidence angle was allow to vary to match lift to vehicle weight, thereby keeping the fuselage level for minimum drag. The rotor shafts were kept level, and the rotors were trimmed to zero flapping with cyclic. The rotors rotate with the lower blades moving inboard, opposite to the swirl in the wing tip vortices.

Twist optimization

The optimum twist distribution varies for different hover/cruise tip-speed ratios and for different mission models. A conventional bilinear twist distribution was used here, with different values of linear twist over the inner and outer blade span. Performance calculations were made for different combinations of inboard and outboard twist for a broad range of cruise tip speeds. CAMRAD II calculated isolated rotor performance at the takeoff hover and long-range cruise conditions of Table 1; the hover tip speed was held fixed at 650 ft/sec and the cruise tip speed was varied from 300-550 ft/sec.

The result is a multidimensional performance map with three independent variables: cruise tip speed (V_{tip}) and inboard and outboard twist rate; and two dependent variables: hover figure of merit (FM) and cruise propulsive efficiency (η). Figure 3 summarizes the performance map as a set of lines denoting the outer boundaries of FM and η at each value of cruise V_{tip}. For each tip speed, the optimum twist will lie somewhere on that line. (The curves in Fig. 3 are slightly different from those in Ref. 13 because the older LCTR2-01 model was updated and revised to the current LCTR2-02 version, as discussed earlier in this paper. The range of tip speeds shown in Fig. 3 is also larger.)

A traditional analysis would feed the values along each boundary into a mission model to compute the lowest fuel burn, hence lowest gross weight. It is immediately evident that 300 ft/sec is too low and 500 ft/sec is too high; the optimum tip speed is 400-450 ft/sec, depending upon the relative importance of hover and cruise performance. However, Fig. 3 alone does not provide enough information to determine the optimum cruise tip speed. Tip speed affects not only performance, but gearbox weight, so a sizing analysis is required.

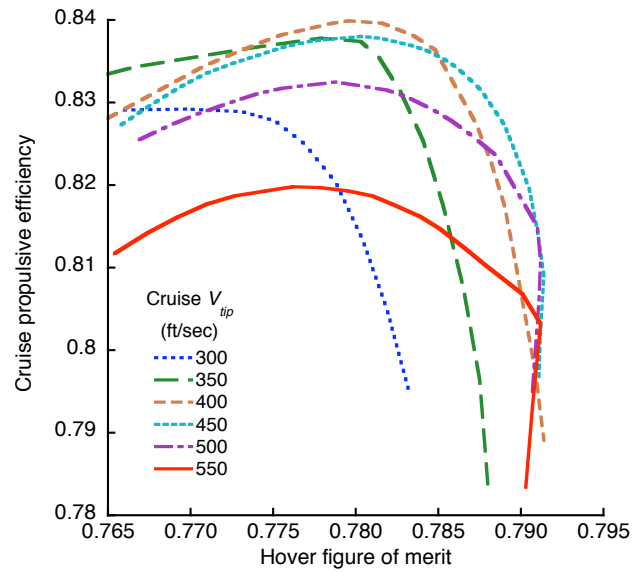

Fig. 3. Boundaries of isolated rotor twist optimizations for different cruise tip speeds.

Rotor/wing interference

To compute rotor/wing interference, the twist combinations along the performance boundary for each tip speed were re-analyzed with CAMRAD II, using a full wing and rotor aerodynamic model (Fig. 2). With two rotors and a wing, each with a wake model and with mutual wing/rotor interference, the performance computations took an order of magnitude longer than for isolated-rotor performance. The large savings in CPU time were the motivation for splitting the CAMRAD II analysis into two series, the first with the isolated rotor model, and the second with the full wing and rotor model.

The full wing/rotor CAMRAD II analysis was done only for cruise; wing/rotor interference in hover was modeled in NDARC by an equivalent vertical drag coefficient, including download. The simpler analysis was appropriate for hover because the hover tip speed is constant and the download model can easily be matched to experimental data or CFD analyses. Equivalent net download was 7.9% for the baseline LCTR2-02.

The performance boundaries shown in Fig. 3 are nonlinear and non-monotonic, as are the variations in twist rates that determine the boundaries. This creates challenges for consistent and unambiguous plotting of the results. For this paper, the convention was adopted that power, weight and other values were usually plotted against hover figure of merit. For a given twist distribution, figure of merit does not vary with cruise tip speed, nor is it affected by cruise wing/rotor interference. Therefore, using figure of merit as the independent variable results in plots with fewer ambiguities and clearer trends (at least to this author's eye). However, weight trends are plotted against both *FM* and η in the NDARC Sizing Analysis section of this paper for contrast.

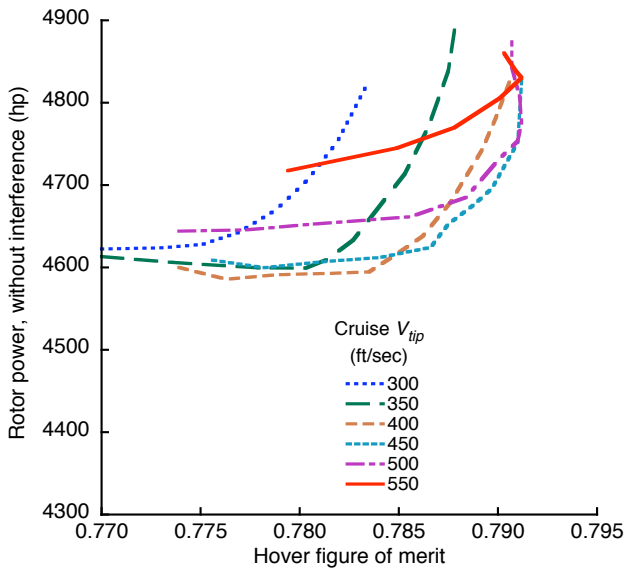

Fig. 4. Rotor power in cruise without wing/rotor interference.

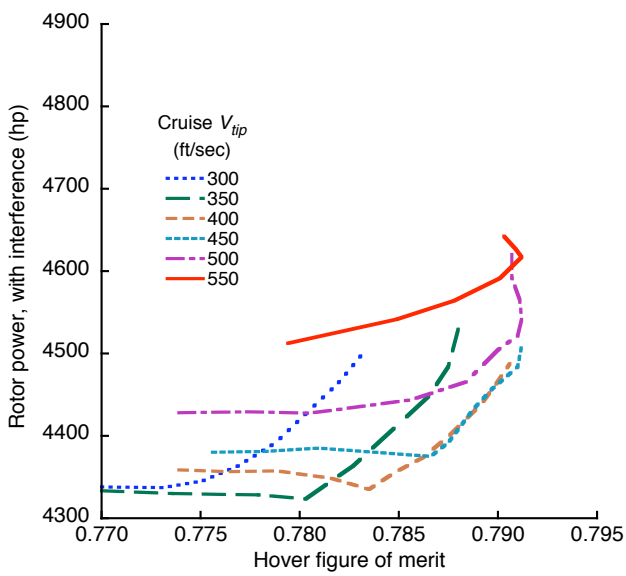

Fig. 5. Rotor power in cruise with wing/rotor interference.

Figures 4 and 5 plot cruise rotor power versus hover figure of merit, the first without, and the latter with rotor/wing interference. The figures in this paper plot the power of only one rotor, not both added together, because that makes for more convenient plot scaling. Figure 4 suggests that any cruise tip speed between 300 and 450 ft/sec will require nearly equal power in cruise. The implication is that profile power and induced power trade off nearly equally as tip speed changes. Figure 5, however, shows that including interference favors the lower tip speeds. The larger swirl losses at V_{tip} = 300-350 ft/sec are offset by greater wing efficiency, as shown in Fig. 6, which plots the change (delta) in wing power caused by interference. Wing power is defined here as wing drag times free-stream velocity. V_{tip} = 350 ft/sec is the optimum value, although 400 ft/sec is nearly as good and gives slightly better hover performance. However, the effects on vehicle sizing have not yet been taken into account.

Figure 6 also plots the change in rotor profile and induced power components caused by interference. Rotor propulsive power has been subtracted out because the change in this power component is equal to the change in wing power. The remaining portion of rotor power (P_o + P_{ind}) is affected much less by interference than wing power.

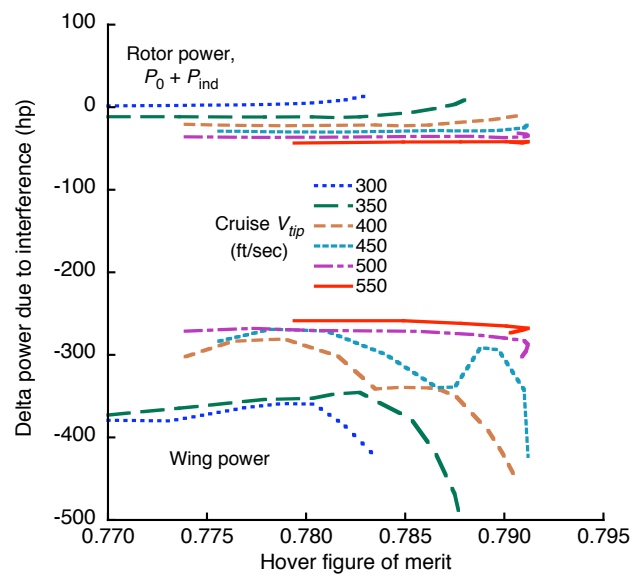

Fig. 6. Changes in wing and rotor power due to interference.

Plots of traditional rotor and wing power and efficiency coefficients are problematic, if for no other reason than the wing and rotor magnitudes differ enormously in scale. Moreover, rotor/wing interference alters some values outside of their traditional range. Kroo (Ref. 19) points out that propeller propulsive efficiency, as traditionally defined, may be greater than one in the presence of

interference. The wing Oswald efficiency factor can also be greater than one because the rotor increases local dynamic pressure above the free-stream value. The approach taken here was to avoid nondimensional power coefficients and plot power components in engineering units, retaining only *FM* and η as nondimensional values on the abscissa. The resulting plots are readable at reasonable scales.

The use of an aeromechanics code such as CAMRAD II allows the rotor and wing drag to be separated into induced, profile, and parasite drag components. This luxury is not possible for wind-tunnel tests, which are necessarily limited in the practical installation of separate rotor and wing balances. For the present study, the rotor was optimized first without interference, and the change in efficiency due to interference was calculated as separate rotor and wing power components. It is important to keep in mind that what matters is the performance of the total wing/rotor system.

Figure 6 also reveals a strongly non-monotonic trend of delta wing power, most evident at V_{tip} = 450 ft/sec. A hook in the curve at high figure of merit is present at nearly all tip speeds, but often difficult to discern at the scale of Fig. 6. It does not appear in the rotor power curves because rotor propulsive power has been subtracted out (it simply mirrors the wing power trends). The trend is caused by the non-monotonic bilinear twist distribution along the rotor performance boundaries (Fig. 3): at high *FM*, the inboard twist rate varies rapidly, but the outboard twist varies slowly or not at all; whereas at high η, the total twist varies slowly as inboard and outboard twist rates vary together, but with opposite trends. The effect can be expected to be different for higher-order rotor optimizations with nonlinear twist distributions.

NDARC Sizing Analysis

To determine the true optimum cruise tip speed, the performance results of Figs. 4-6 were fed into NDARC and the LCTR2 resized. Instead of using only figure of merit and propulsive efficiency, the rotor performance was modeled in NDARC with equivalent profile drag c_{do} and induced power factor κ (the ratio of induced velocity to the ideal induced velocity from momentum theory). The hover and cruise performance models used separate values of c_{do} and κ, generated by the CAMRAD II analyses. The effect of interference on wing performance was modeled in NDARC by varying the Oswald efficiency factor *e*. κ and *e* are defined as follows:

$$P_{ind} = \kappa T v_i \ , \ v_i = \sqrt{T/2\rho A} \qquad \text{(Ref. 1)}$$

$$e = \frac{1}{\pi b^2}\frac{(L/q)^2}{D_i/q} \qquad \text{(Ref. 11)}$$

These inputs are, in effect, nondimensional representations of the power variations in Figs. 4-6. The wing incidence angle was also varied to match that calculated by CAMRAD II. The results are plotted in Figs. 7-10.

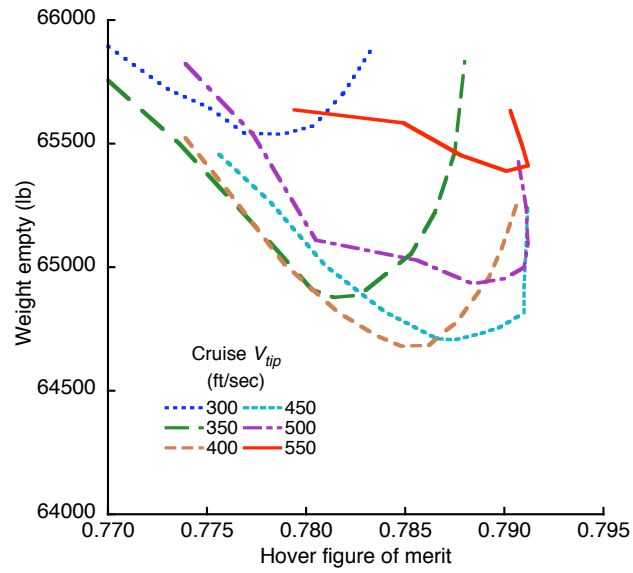

Fig. 7. Weight empty, without interference.

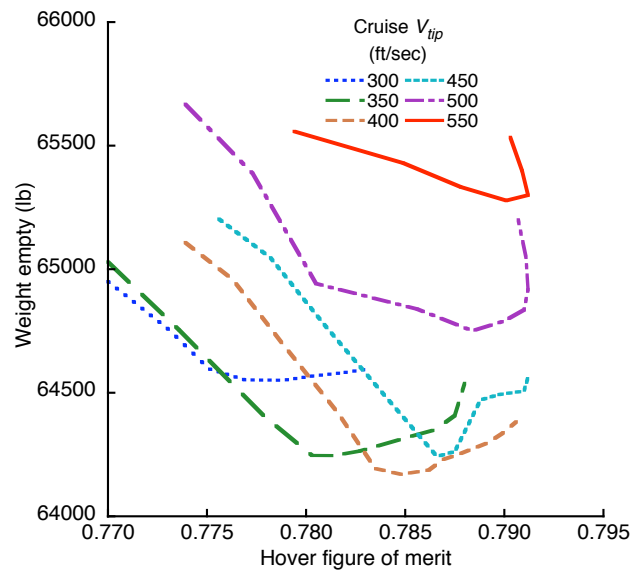

Fig. 8. Weight empty, with wing/rotor interference.

Figures 7 and 9 show that the weight-optimized cruise tip speed is somewhat higher than that determined from rotor power alone (Figs. 3 and 4). Figures 8 and 10 replot weight empty against η. Without interference, the optimum V_{tip} is 400-450 ft/sec; with interference, the range extends to 350-450 ft/sec. The optimum value is also more sensitive to the twist distribution, as is most evident in Fig. 8, which clearly shows separate minima for each tip speed. Contrast with Fig. 4, which shows broad, nearly flat minima. A proper sizing analysis is

needed to determine the true optimum tip speed and corresponding twist distribution. Table 4 summarizes the results of the sizing analysis for those cruise tip speeds yielding the lowest empty weights.

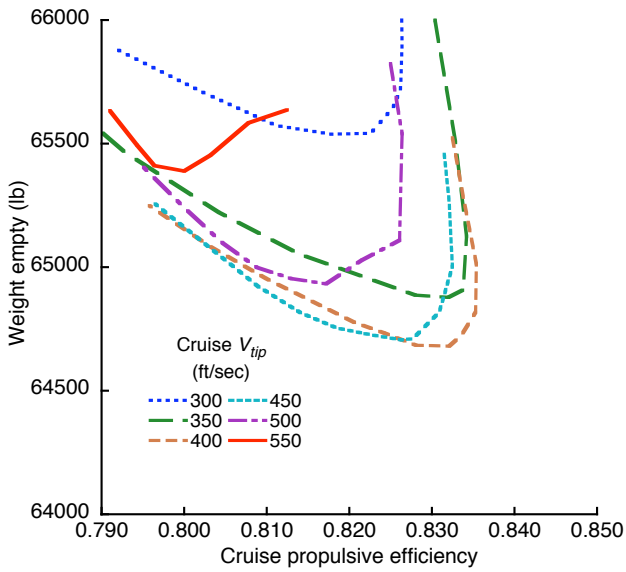

Fig. 9. Weight empty, without interference.

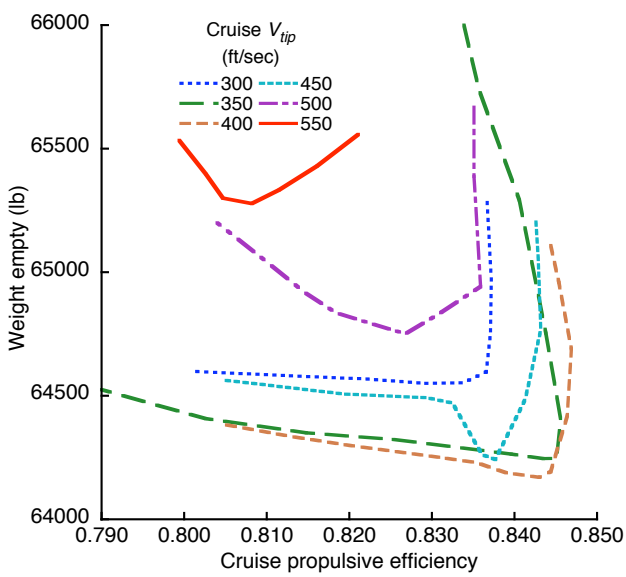

Fig. 10. Weight empty, with wing/rotor interference.

Table 4. Summary results for minimum empty weight.

Cruise V_{tip} (ft/sec)	Cruise M_{tip}	FM*	η*	Twist (deg)	WE (lb)
350	0.3488	0.7814	0.8435	36.3	64246
400	0.3986	0.7848	0.8430	40.4	64170
450	0.4485	0.7866	0.8377	42.6	64242

* Values for isolated rotor (compare Fig. 3)

The most practical choice would favor the cruise V_{tip} with the highest FM and η, consistent with low weight; Figs. 8 and 10 show this value to be near 400 ft/sec. This choice may easily change as new technology, such as purpose-designed airfoils, is folded into the LCTR2 design.

Figure of merit is linked to cruise V_{tip} through the twist distribution. A multi-panel twist optimization would doubtless have resulted in a more precise end result than that reported here for bilinear twist. However, the more elaborate performance analyses required would have taken substantially more CPU time. During development of the coupled aeromechanics/sizing method, it proved useful to periodically check the underlying physics of the aeromechanics analysis, notably the circulation distribution, for reasonable behavior. Use of relatively simple twist distributions facilitated such checks. Once the procedures have been fully developed and a robust baseline design chosen, it would then be appropriate to perform higher-order optimizations. These would include more elaborate twist distributions, nonlinear taper, tip extension geometry, etc. for the rotor and airframe, and may include alternative missions, such as maximum-range ferry, STOL takeoff, etc.

Lessons Learned

During the development of the procedures described here, several lessons were learned concerning the appropriate levels of accuracy and other numerical issues of the aeromechanics analyses. Some of the lessons were already known, or at least are obvious in retrospect, but the details of implementation in CAMRAD II had to be worked out for the LCTR2 configuration. Different codes will have different ways of implementing circulation, trim and wake tolerances, probably with different reference values for each. The following observations will have to be interpreted accordingly.

Circulation in cruise: In cruise, the total inflow and dynamic pressure are so high that tiny changes in trim settings can cause large changes in thrust. It is not enough to trim to a small tolerance on thrust: the entire lift (and drag) distribution must be well-converged, or else the resulting power will be inaccurate. In CAMRAD II, this is best achieved by imposing a very tight tolerance on circulation, which must be significantly smaller in cruise than in hover, typically by a ratio of 1/5.

Rotor and wing trim: Additional constraints are imposed when analyzing the rotors and wing together. The wing lift is much larger than the rotor thrust. With two rotors, the ratio of wing lift to single-rotor thrust is twice the total lift-to-drag ratio. The trim tolerances on wing lift and rotor thrust must each be scaled accordingly. The force tolerances (thrust or lift) may have to be further adjusted if rotor/wing interference is included. It is

usually more difficult to trim the rotor than the wing, especially if rotor flapping is explicitly trimmed. For these reasons, the analysis used a single, global force tolerance referenced to rotor thrust, based on the observation that if rotor forces are properly trimmed, then trimming the wing lift to the same tolerance will be more than adequate.

Wake convergence: In hover, convergence of the wake becomes an issue. The wake model in CAMRAD II is computationally expensive and is, therefore, the outermost loop of the analysis. Wake distortion and circulation are converged during inner loops, but there is no internal convergence test for the outer wake loop (Ref. 4). For the analyses done here, the critical results were hover figure of merit and cruise propulsive efficiency. Neither of these are trim parameters, nor were the underlying values of c_{do} or κ. There was no metric on wake convergence, referenced to these parameters, equivalent to trim convergence on rotor or airframe forces. The critical trim, wake, and efficiency parameters are computed within different loops, making it difficult to define a single, global convergence criterion.

In past efforts (e.g. Refs. 13 and 17), this problem was greatly alleviated by computing the entire matrix of any given parameter variation (twist, taper, etc.). It may seem paradoxical that computing a large set of variations may be more efficient, and even more accurate, than using formal optimization to converge on the optimal values. The key is that the path through the parameter matrix may be chosen in advance to facilitate convergence and thereby reduce total computational time. CAMRAD II allows the wake geometry and flow solution for one case to be applied to the next case of rotor variations. For small changes in rotor parameters, subsequent cases converge very quickly. In fact, it was sometimes more efficient to introduce additional cases to pre-converge the solution than to run more wake iterations. Careful checks of wake convergence, and of any other global or outer-loop computations, must be done in advance of any design optimizations. This is particularly important when running an automatic optimizer that discards portions of the parameter matrix or otherwise shrinks the design space to save computational time, because important clues to convergence problems may be lost.

In cruise, the wake converges much faster than in hover, even with rotor/wing interference. The issues just discussed for hover were not seen for the cruise computations in this study (but that does not guarantee that they will not occur in future analyses).

Observations and Recommendations

Integrated aeromechanics analysis and vehicle sizing (weight optimization) was demonstrated with the CAMRAD II aeromechanics code and NDARC sizing code. The example was optimization of cruise tip speed with rotor/wing interference for the LCTR2 tiltrotor concept design.

Although a minimum-weight design can be determined from the results presented here, the most telling result is that optimum weight varies little over a range of cruise tip speeds, roughly 350-450 ft/sec. The range of acceptable tip speeds is not evident when comparing weight trends computed without taking wing/rotor interference into account. Performance trends alone are insufficient, even when interference is included: a sizing analysis is needed to identify the optimum range of tip speeds. These trends will doubtless change as new technology is included into the design, or if the mission is revised.

Perhaps a more subtle result is that the process of choosing airfoil, planform, twist and other design variables may benefit from revision. Instead of narrowing the design space to a single, best cruise tip speed, the results expand the range of tip speeds at which other design variables must be analyzed. This increases the burden on the designer to investigate a larger matrix of variables, but with the payoff of a better design than could be obtained otherwise—the classic challenge of multidimensional design optimization.

At the least, more sophisticated component design methods should be applied to determine the true optimum cruise tip speed. An obvious example is that the tradeoffs between airfoil performance characteristics—minimum drag, maximum lift, pitching moment, etc.—will determine the optimum cruise tip speed, instead of a single tip speed determining the airfoil design. In parallel, a nonlinear, multi-segment blade twist distribution may be needed. There remains the requirement to explicitly include maneuvering flight conditions in the coupled aeromechanics and sizing optimization.

Acknowledgements

The author wishes to acknowledge the assistance of Dr. Hyeonsoo Yeo of the U. S. Army Aeroflightdynamics Directorate at Ames Research Center, who provided the wing/rotor wake model, and the generous advice of Dr. Wayne Johnson of NASA Ames Research Center, who developed both CAMRAD II and NDARC.

References

1. Johnson, W., "NDARC—NASA Design and Analysis of Rotorcraft: Theoretical Basis and Architecture," AHS Aeromechanics Specialists' Conference, San Francisco, California, January 2010.

2. Johnson, W., "NDARC, NASA Design and Analysis of Rotorcraft," NASA TP 2009-215402, December 2009.

3. Johnson, W., Rotorcraft Aerodynamics Models for a Comprehensive Analysis, 54th Annual Forum of the American Helicopter Society, Washington, D.C., 1998.

4. Johnson, W., "CAMRAD II Comprehensive Analytical Model of Rotorcraft Aerodynamics and Dynamics," Johnson Aeronautics, Palo Alto, California, 2005.

5. Johnson, W., Yamauchi, G. K., and Watts, M. E., "NASA Heavy Lift Rotorcraft Systems Investigation," NASA TP-2005-213467, September 2005.

6. Johnson, W., Yamauchi, G. K., and Watts, M. E., "Designs and Technology Requirements for Civil Heavy Lift Rotorcraft," AHS Vertical Lift Aircraft Design Conference, San Francisco, California, January 2005.

7. van Aken, J. M. and Sinsay, J. D., "Preliminary Sizing of 120-Passenger Advanced Civil Rotorcraft Concepts," AHS Vertical Lift Aircraft Design Conference, San Francisco, California, January 2006.

8. Acree, C. W., and Johnson, W., "Performance, Loads and Stability of Heavy Lift Tiltrotors," AHS Vertical Lift Aircraft Design Conference, San Francisco, California, January 2006.

9. Acree, C. W., Martin, P. B., and Romander, E. A., "Impact of Airfoils on Aerodynamic Optimization of Heavy Lift Rotorcraft," AHS Vertical Lift Aircraft Design Conference, San Francisco, California, January 2006.

10. Acree, C. W., "Impact of Technology on Heavy Lift Tiltrotors," 62nd Annual Forum of the American Helicopter Society, Phoenix, Arizona, May 2006.

11. Yeo, H., and Johnson, W., "Performance and Design Investigation of Heavy Lift Tiltrotor with Aerodynamic Interference Effects," 63rd Annual Forum of the American Helicopter Society, Virginia Beach, Virginia, May 2007.

12. Johnson, W., Yeo, H., and Acree, C.W., "Performance of Advanced Heavy-Lift, High-Speed Rotorcraft Configurations," AHS International Forum on Rotorcraft Multidisciplinary Technology, Seoul, Korea, October 2007.

13. Acree, C. W., Yeo, H., and Sinsay, J. D., "Performance Optimization of the NASA Large Civil Tiltrotor," International Powered Lift Conference, London, UK, July 2008; also NASA TM-2008-215359, June 2008.

14. Acree, C. W. Jr. and Johnson, W., "Aeroelastic Stability of the LCTR2 Civil Tiltrotor," AHS Technical Specialists' Meeting, Dallas, Texas, October 15-17, 2008.

15. Yeo, H., Sinsay, J. D., and Acree, C. W., "Blade Loading Criteria for Heavy Lift Tiltrotor Design," AHS Technical Specialists' Meeting, Dallas, Texas, October 15-17, 2008.

16. Preston, J., and Peyran, R., "Linking a Solid-Modeling Capability with a Conceptual Rotorcraft Sizing Code," AHS Vertical Lift Aircraft Design Conference, San Francisco, California, January 2000.

17. Acree, C. W., "Modeling Requirements for Analysis and Optimization of JVX Proprotor Performance," 64th Annual Forum of the American Helicopter Society, Montréal, Canada, April 2008; also NASA TM-2008-214581, May 2008.

18. McVeigh, M. A., Grauer, W. K., and Paisley, D. J., "Rotor/Airframe Interactions on Tiltrotor Aircraft," *Journal of the American Helicopter Society*, Vol. 35, No. 3, July 1990.

19. Kroo, I., "Propeller-Wing Integration for Minimum Induced Loss," *Journal of Aircraft*, Vol. 23, No. 7, July. 1986.

20. Snyder, M. H., and Zumwalt, G. W., "Effects of Wingtip-Mounted Propellers on Wing Lift and Induced Drag, *Journal of Aircraft*, Vol. 6, No. 5, September-Oct. 1969.

21. Miranda, L. R., and Brennan, J. E., "Aerodynamic Effects of Wingtip-Mounted Propellers and Turbines," AIAA 86-1802, 1986.

22. Witkowski, D. P., Lee, A. K. H., and Sullivan, J. P., "Aerodynamic Interaction Between Propellers and Wings," *Journal of Aircraft*, Vol. 26, No. 9, September 1989.

23. Deckert, W. H., and Ferry, R. G., "Limited Flight Evaluation of the XV-3 Aircraft," Air Force Flight Test Center Report AFFTC-TR-60-4, May 1960.

24. Corrigan, J. J., and Schillings, J.J., "Empirical Model for Stall Delay Due to Rotation," AHS Aeromechanics Specialists Conference, San Francisco, California, January 1994.

25. Narramore, J. C., "Airfoil Design, Test, and Evaluation for the V-22 Tilt Rotor Vehicle," 43rd Annual Forum of the American Helicopter Society, St. Louis, Missouri, May 1987.